

Domain wall dynamics in stepped magnetic nanowire with perpendicular magnetic anisotropy

S. Al Risi¹, R. Sbiaa^{1*} and M. Al Bahri²

¹Department of Physics, Sultan Qaboos University, P.O. Box 36, PC 123, Muscat, Oman

²Department of Basic Sciences, A'Sharqiyah University, Post Box 42, PC 400, Ibra, Oman

Corresponding Email id: * rachid@squ.edu.om

Abstract

Micromagnetic simulation is carried out to investigate the current-driven domain wall (DW) in a nanowire with perpendicular magnetic anisotropy (PMA). A stepped nanowire is proposed to pin DW and achieve high information storage capacity based on multi-bit per cell scheme. The DW speed is found to increase for thicker and narrower nanowires. For depinning DW from the stepped region, the current density J_{dep} is investigated with emphasis on device geometry and materials intrinsic properties. The J_{dep} could be analytically determined as a function of the nanoconstriction dimension and the thickness of the nanowire. Furthermore, J_{dep} is found to exponential dependent on the anisotropy energy and saturation magnetization, offering thus more flexibility in adjusting the writing current for memory applications.

Keywords: Magnetic nanowires, perpendicular magnetic anisotropy, domain wall motion, spin transfer torque

1. Introduction

Magnetic random access memory (MRAM) gained attention as a possible replacement to conventional memories such as static and dynamic RAMs and even flash memory. It has several advantages as reported in few articles [1–6]. For the MRAM device based on magnetic tunnel junctions (MTJs), the direction of magnetization defines the magnetic state, thus only one bit per cell could be stored. For increasing the storage capacity of the memory, there were attempts to use MTJs with two free layers to achieve four magnetic states [7,8]. For even more storage capacity, domain wall (DW)-based MRAM was intensively investigated [9–21]. The first generation of DW-based devices was based on materials with in-plane magnetic anisotropy (IMA). However, the continuous reduction of device size makes these materials less effective in keeping the magnetic state (information) stable. On the other hand, materials with perpendicular magnetic anisotropy (PMA) have the advantage to provide better thermal stability due to the higher magnetic anisotropy.

Different studies have been focused on domain wall movement in nanowires with in-plane anisotropy and an emphasis on the dependence of the velocity of DW on nanowire dimensions. It has been reported that DW motion can be controlled by adjusting the nanowire width and thickness [22,23]. For in-plane (IMA) material, DW velocity could be made larger by increasing nanowire width and decreasing its thickness.

To store the information in magnetic domains, the DW should be stable at a predefined position within the nanowire. Pinning DW at a precise position has been

investigated with several schemes [26-27]. One of them was based on creating triangular notches with different geometries for DW made of permalloy material [24-27]. Another way like using a magnetic field perpendicular to the direction of DW motion to reduce the speed of DW to zero at a required position was also proposed [28]. In such a method, the magnetic field needed to pin DW is higher than the Walker field and causes deformation for the DW structure.

In our previous work, we proposed nanowire with a stepped area to pin DW in materials with in-plane magnetic anisotropy [23,29]. In this paper, we focus on material with perpendicular anisotropy and we used micromagnetic formalism with the inclusion of spin-transfer torque effect with both adiabatic and non-adiabatic terms.

2. Theoretical model

In this study, we investigate a magnetic nanowire of fixed length $L = 200$ nm and varied width w and thickness t_z as shown in Fig.1(a). The device is divided into small meshes with the size of $(2.5 \times 2.5 \times t_z)$ nm³. The size of the mesh is chosen to be smaller than the exchange length l_{ex} of the materials considered in this study. In the last part, the saturation magnetization (M_s), the perpendicular magnetic anisotropy (K_u) are varied while the exchange length (A) was kept constant ($A = 2 \times 10^{11}$ J/m). These chosen values correspond to the actual magnetic properties of the Co/Ni multilayers as reported previously [30]. The calculation is carried out with the object-oriented micromagnetic framework (OOMMF) based on the Landau-Lifshitz-Gilbert (LLG) equation with spin-transfer torque (STT) term [31].

$$\begin{aligned} \frac{d\mathbf{m}}{dt} = & -\gamma(\mathbf{H}_{\text{eff}} \times \mathbf{m}) + \alpha(\mathbf{m} \times \frac{d\mathbf{m}}{dt}) \\ & + \mathbf{u} \times \left(\mathbf{m} \times \frac{\partial \mathbf{m}}{\partial t} \right) + \beta \cdot \mathbf{u} \cdot \mathbf{m} \\ & \times \frac{\partial \mathbf{m}}{\partial t} \end{aligned} \quad (1)$$

where \mathbf{m} is the normalized magnetization vector, γ is the gyromagnetic ratio, α is the Gilbert damping parameter, the vector $\mathbf{u} = (gP\mu_B/2eM_s)\mathbf{J}$ is the adiabatic spin torque which has the dimension of velocity, J is the current density, g is the Lande factor, P is the spin polarization, e is the charge of electron and μ_B is the Bohr magneton. In the middle of the nanowire, a stepped junction is designed by shifting one part in the x -direction and the other in the y -direction, called λ and d , respectively to pin DW [Fig.1 (b)]. Initially, the magnetic moments are saturated in z -direction then the domain wall was created at the left edge of the nanowire so the DW could move easily under a reasonably low current density. The DW could be pinned at the stepped region, then at a certain value of current density, the DW is released. This critical current density is called the depinning current density (J_{dep}). The calculations are performed by using LLG equation. Different values of the width and thickness of the nanowire were chosen to explore the dependence of DW velocity and the depinning current on device geometry. The dimensions of the stepped area is also varied. Fig. 1(a) shows the conventional nanowire while Fig. 1(b) illustrates the proposed stepped type which is efficient in pinning/ stabilizing DW for memory applications.

3. Results and Discussion

In this study, all magnetic moments within the

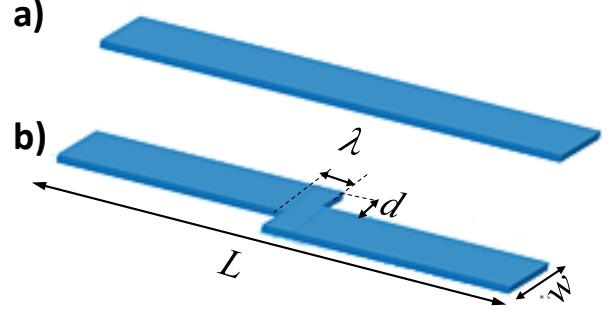


Figure 1. (a) Conventional nanowire with length L and width w and (b) Nanowire with a stepped area at its center with dimensions d and λ to pin the DW.

nanowire are initially considered aligned in the negative z -direction (perpendicular to the nanowire plane). The spin-polarized current was then applied from the left edge of the nanowire to the right edge along the x -direction perpendicular to the direction of magnetization. Firstly, the simulations are performed using a conventional nanowire without any stepped region to investigate the DW dynamics as shown in Fig. 1 (a). In this case, DW is created as an initial state at nanowire left edge and moves through the nanowire without observing any pinning within the device as shown in Fig.2 (a). The motion of DW from the initial state ($m_z = -1$) to the final state ($m_z = +1$) happens with constant velocity as shown by the linear dependence of m_z with time ($m_z = M_z/M_s$ is the normalized z -component of the magnetization). The insets of Fig. 1(a) are captured images showing a temporary displacement of DW along the nanowire. Fig. 2(b) shows the plots of DW velocity v as a function of J for different widths of the nanowire. It is found that v has a linear dependence with J , similar to what was reported by several groups for nanowires with

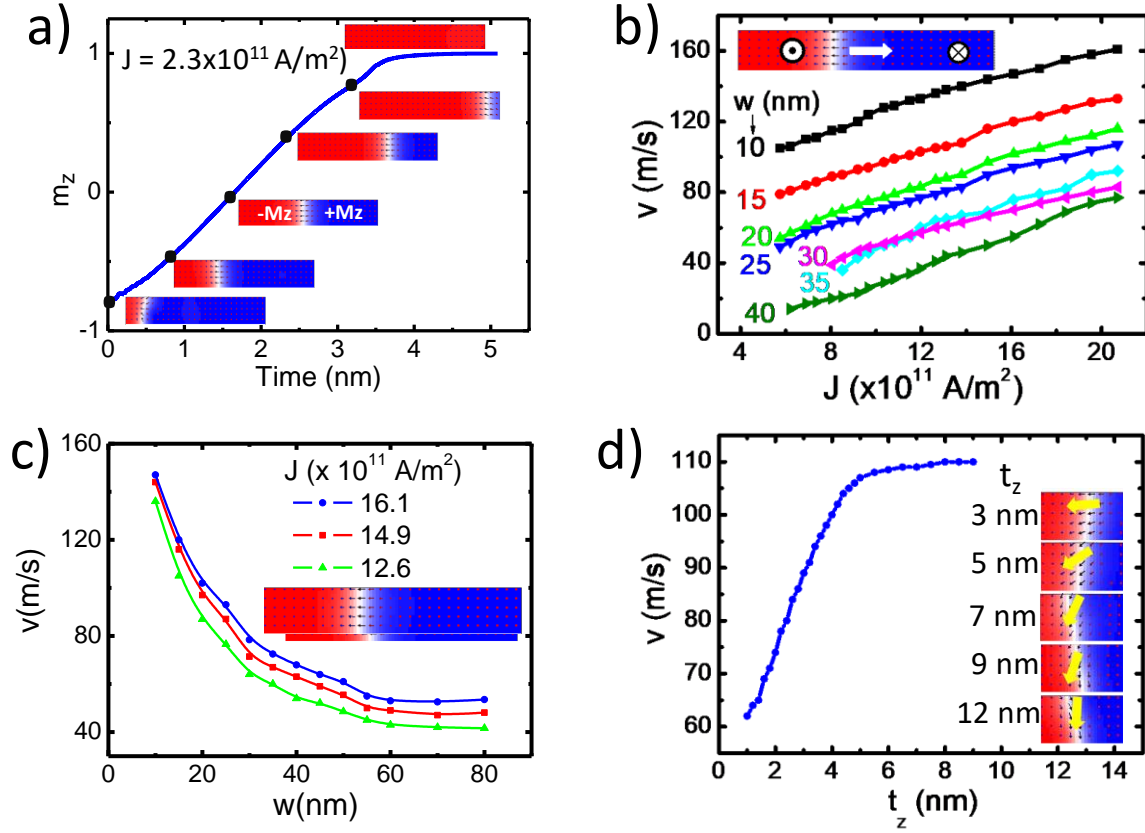


Fig. 2. (a) Normalized magnetization of a conventional nanowire as a function of time for device with $L=200$ nm, $w = 40$ nm, $M_s = 802 \times 10^3$ A/m, $K_u = 5.3 \times 10^5$ J/m³, $A = 2 \times 10^{11}$ J/m and $J = 23 \times 10^{11}$ A/m² (b) plot of the DW average velocity as a function of current density for various nanowire widths. (c) DW average velocity as a function of the width of conventional nanowire for various applied current density values and (d) a plot of the average velocity and the conventional nanowire thickness for $J = 23 \times 10^{11}$ A/m². Insets are snapshots of magnetic moments at the vicinity of DW showing the transformation from Néel wall to Bloch wall.

PMA [13,32–35]. The velocity versus current density could be described by

$$v = \frac{\varepsilon \gamma \hbar P}{2eM_s \alpha} J \quad (2)$$

where \hbar is the reduced Planck constant and ε is the non-adiabatic parameter [32,36].

For a device with 10 nm width, the velocity rose from 110 m/s (at a current density of

6×10^{11} A/m²) to 160 m/s (at a current density of 20×10^{11} A/m²). We confirmed this result by investigating the influence of nanowire width on the dynamics of DW. From Fig. 2(c), it could be seen that the DW velocity increases as nanowire is made narrow following the relation $J = i/w\Delta$. The equation (2) becomes,

$$v = \frac{\varepsilon \gamma \hbar P i}{2eM_s \alpha w \Delta} \quad (3)$$

where i the current flows, w is the nanowire width and Δ is the DW width [35].

It has been argued that as the nanowire width becomes smaller, the hard axis anisotropy field decrease and the Néel wall becomes more stable, therefore the current density enhances the DW dynamics [37]. The other key parameter which has a strong effect on DW dynamics is the nanowire thickness. Fig. 2(d) is a plot of the dependence of v on t_z . Insets are the domain wall configuration for different nanowires thicknesses it is found that the velocity has an almost linear dependence on the thickness for a certain range of values (t_z between 1 and 6 nm) and agrees with the relation,

$$v = \frac{0.01\gamma a_J t_z}{\alpha} \quad (4)$$

where $a_J = \hbar J P / 2 t_z e M_s$ [36]. In this study, a current density of 23×10^{11} A/m² was applied and t_z was varied from 1 nm to 12 nm while the other parameters were kept constant. It can be seen that DW velocity increases rapidly as thickness varied from 1 nm to 5 nm to reach a velocity of about 110 m/s for a device with 5 nm thickness. It can also be seen from Fig. 2 (d) that the velocity did not change much for large thickness (more than 5 nm). As the thickness varies, the micromagnetic simulation shows the transformation from a Néel wall to Bloch wall [insets of Fig. 2 (d)]. This could be the reason for the fast increase of the velocity with thickness.

For the use of the stepped nanowire as a memory device, the effect of the stepped region dimension of the depinning current density is of great importance. There is a balance between the stability of the domain wall and the minimum J_{dep} needed to move it to the next step

(i.e., state). Firstly, the DW is created in the left edge of stepped nanowire and the current is applied to move the DW. Once the DW is stabilized/pinned in the stepped region, considered as the initial state, the current was varied continuously until it is depinned. The depinning current density was investigated for stepped nanowires with widths of values changing from 20 nm to 60 nm with a step of 0 nm while the length of the step (d) was fixed to ($w/2$). From Fig. 3 (a), it can be seen that for $w = 20, 30$ and 40 nm, J_{dep} decreases exponentially with λ . For larger values of w an almost linear behavior was observed. The geometry of the stepped region provides an easy way to adjust the pinning strength for stabilizing DW at a defined position. By enlarging its lateral size (λ), DW can be depinned more easily. Fig. 3(b) shows the dependence of J_{dep} on the thickness of the device for different values of d . The most striking result to emerge from the data is that J_c increases with the thickness for different values of d (here λ was fixed to zero). Hence with these interesting results, we can achieve a higher depinning current and higher speed with larger thickness and narrow nanowire. The numerical data obtained from LLG equation can be described analytical using the expression $J_{dep} = A + B e^{-\lambda/\xi}$. Here λ is the length of nano-constriction in the x -direction and ξ is a fitting parameter as well as A and B . The values of ξ for different nanowire widths w are summarized in Tab. 1. It is important to mention that for small values of w , J_{dep} shows a linear behavior with λ as can be seen in Fig. 3(a). By looking carefully at Fig. 3(b), it can be seen that J_{dep} has an exponential growth with the nanowire thickness. In this case, the depinning current density can be expressed as

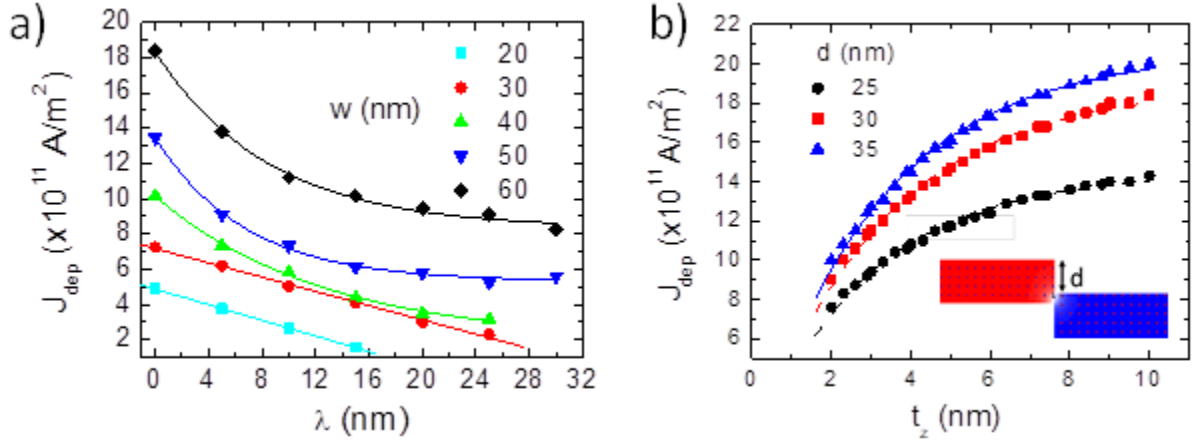


Figure 3. (a) Plots of J_{dep} versus the step width λ for various widths of nanowire w . For the plots, d was fixed to $w/2$. (b) J_{dep} versus the nanowire thickness t_z for $d = 25, 30$ and 35 nm and $\lambda = 0$.

$J = J_0(1 - e^{-\rho t_z})$. In the same manner as in Fig. 3(a), the parameters J_0 and ρ , which are reported in Tab. 2, could be obtained for different values of d (the nanoconstriction size along y -direction). From table 2, one could see that the fitting parameter ρ is not much dependent on d in the investigated range. The parameter J_0 , which is considered as the current density for relatively thick nanowire, is continuously increasing with d as expected. In fact, J_{dep} is higher for large values of d for any nanowire thickness value [Fig. 3(b)]. After investigating the effect of device geometry on the dynamics of DW and the depinning current

Tab. 1. The dependence of the fitting parameters ξ and B on the width of the nanowire. The device dimensions and materials properties as taken from Fig. 3(a)

w (nm)	ξ (nm)	$B(\times 10^{11} \text{ A/m}^2)$
40	12.6 ± 1.0	8.2 ± 0.3
50	6.8 ± 0.5	8.1 ± 0.2
60	8.5 ± 0.7	10.0 ± 0.3

density, the study focused on the effect of the key material properties such as M_s and K_u on J_{dep} . Firstly, M_s was fixed while K_u was varied between 5.0×10^5 and $10.0 \times 10^5 \text{ J/m}^3$. In this calculation, DW was first brought to the stepped region then current was applied to depin it from its initial position. Fig. 4(a) is a plot of J_{dep} as a function of K_u for different values of d (λ was fixed to 0 nm). Here, the saturation magnetization was fixed to 800kA/m. It was found that the values of J_{dep} obtained from numerical calculation using LLG equation could be fitted to an exponential growth function $\exp(K_u/t_1)$. The parameter t_1 is a fitting parameter that has the dimension of

Tab. 2. The fitting parameters taken from exponential growth function and plotted in Fig. 3(b) for different values of d .

d (nm)	ρ (nm ⁻¹)	$J_0(\times 10^{11} \text{ A/m}^2)$
25	0.350 ± 0.006	14.5 ± 0.1
30	0.307 ± 0.005	18.9 ± 0.1
35	0.311 ± 0.004	20.6 ± 0.1

energy. From the best fit, t_1 is found to be almost constant for $d = 30$ and 35 nm with values of 6.9×10^5 and 7.0×10^5 J/m³, respectively. A slightly larger drop of t_1 to 4.5×10^5 J/m³ was obtained for $d = 25$ nm. Similarly, the effect of M_s on J_{dep} was investigated. It can be seen from Fig. 4(b) that under the same device geometry, J_{dep} shows, in contrast, an exponential decay (1st order) with M_s for a constant K_u . The plots in Fig. 4(b) are for $K_u = 5.3 \times 10^5$ J/m³. The J_{dep} can be described by the function $\exp(-M_s/t_2)$ where t_2 is a fitting parameter with values of 345, 656 and 1166 kA/m for $d = 25, 30$ and 35 nm, respectively. Optimizing J_{dep} is essential for memory applications. It should be reasonably low in order to move the DW from one step to the other with a low applied current, i.e., changing the magnetic state by displacing DW within the nanowire. One can design the nanoconstriction dimensions for different values of K_u and M_s as described analytically above by the growth and the decay functions, respectively.

For the evaluation of the influence of K_u on DW stability and its magnetic configuration in the vicinity of the stepped area, we conducted the calculation of time dependence of the magnetization for three values of K_u . Figures 5(a) and (b) show snapshot images of the nanowire with $K_u = 5 \times 10^5$ J/m³ and 10×10^5 J/m³ (M_s was fixed to 800 kA/m). These are typical values for Co/Pt, Co/Ni, Co/Ni/Co/Pt multilayers and CoFeB commonly used for magnetic materials with perpendicular anisotropy [30,38–43]. The device dimensions including the nanoconstriction size are $L = 200$ nm, $w = 40$ nm, $d = 35$ nm and $\lambda = 10$ nm. The calculation was carried with a current density of 4.1×10^{11} A/m². Although DW could be stabilized in the stepped area, it will not remain for a long time. Fig. 5(c), shows that DW takes less than 5 ns before vanishing; i.e., moving to the right edge of the device. To overcome this issue, an increase of K_u is necessary, which has been demonstrated for $K_u = 10 \times 10^5$ J/m³.

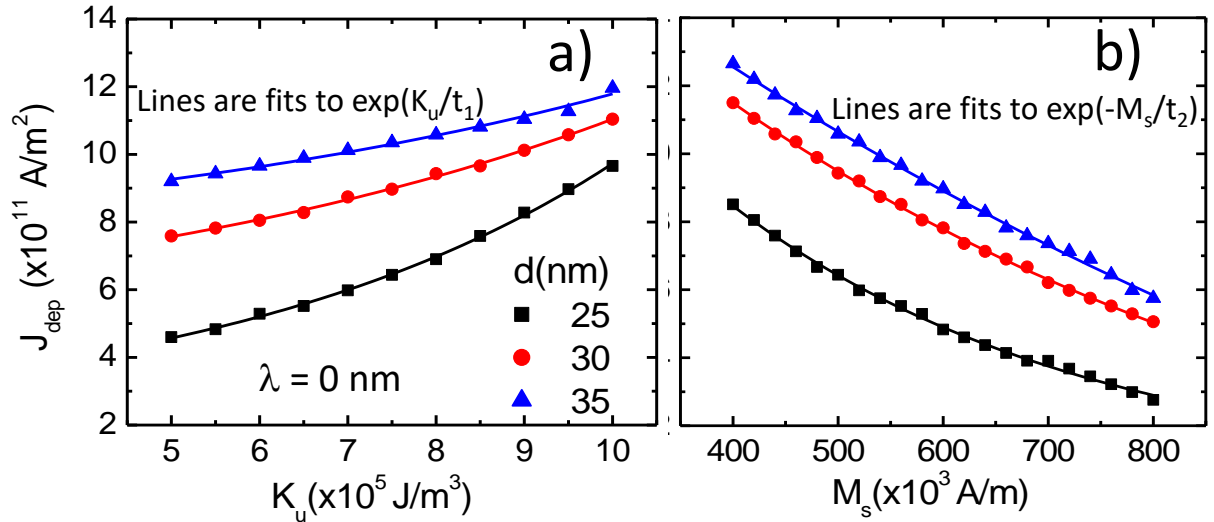


Figure 4. Domain wall depinning current density versus (a) K_u and (b) M_s for different values of d . The lines are fit to exponential growth function for case (a) and exponential decay for case (b). The nanowire length and width are fixed to 200 nm and 40 nm, respectively.

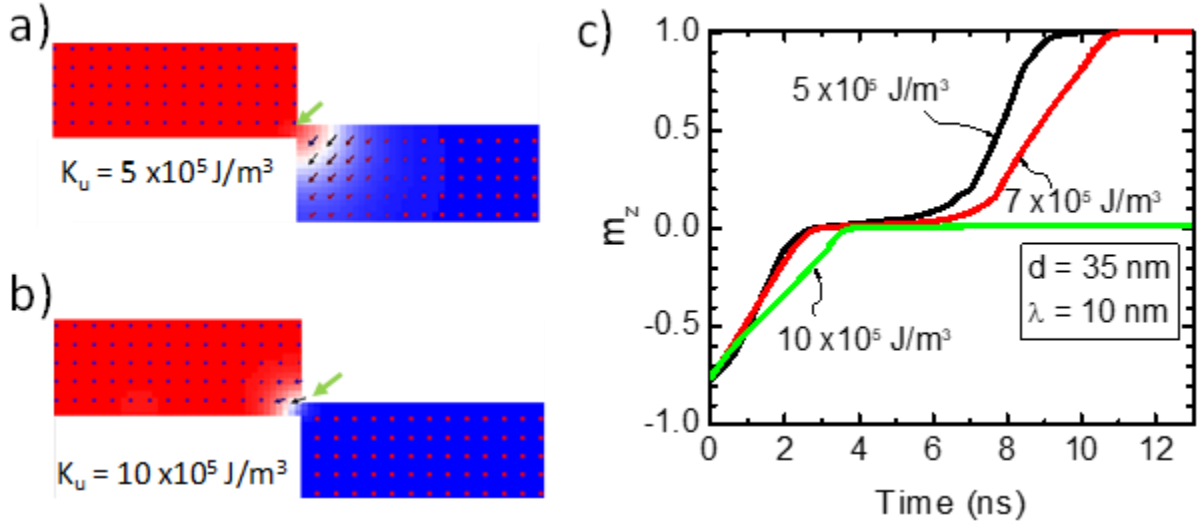


Figure 5. (a) Snapshot images of the nanowire near the stepped area for $K_u = 5.0 \times 10^5 \text{ J/m}^3$ and $5.5 \times 10^5 \text{ J/m}^3$. The length and width of the nanowire are fixed to 200 nm and 40 nm, respectively and the stepped region dimensions d and λ are fixed to 35 nm and 10 nm, respectively. The calculation is conducted for $M_s = 800 \text{ kA/m}$ and $J = 4.1 \times 10^{11} \text{ A/m}^2$. (b) Normalized magnetization in z -direction versus time for three values of K_u (4.5×10^5 , 5.0×10^5 and $5.5 \times 10^5 \text{ J/m}^3$).

It is important to mention that it is also possible to stabilize DW at the stepped region for relatively low K_u by enlarging d or shrinking λ . We noticed that magnetic moments configuration near the stepped area changes with K_u (Fig. 5).

The dynamics of DW at the stepped area based on the influence of M_s was also investigated. In the same manner, DW could be stabilized at the nanoconstriction for small values of M_s .

The stepped type nanowire offers an easy and accurate way of pinning DW within the device. In addition to the nanoconstriction dimension, the material magnetic properties, such as M_s and K_u , provide a further degree of freedom to lower the depinning current density and stabilizing the DW for high capacity memory applications.

4. Conclusion

Domain wall dynamics was investigated in magnetic nanowires with perpendicular anisotropy. A comparison between conventional and stepped nanowires was carried out. In the first scheme, the velocity showed a linear increase with the current density and dropped exponentially with the device width. In the stepped nanowire scheme, it was found that for particular dimensions of the nanoconstriction region, DW could be stabilized and pinned. The dependence of depinning current density J_{dep} on the thickness of the nanowire and dimensions of the stepped region could be described analytically. Furthermore, the dependence of J_{dep} on the material properties was studied. The J_{dep} could also be fitted analytically by either an

exponential growth or exponential decay functions with K_u and M_s , respectively. Tuning and predicting analytically the device geometry and materials properties for an optimal J_{dep} is important for designing DW-based memory devices.

References

- [1] Wolf S. A., Awschalom D. D., Buhrman R. A., Daughton J. M., Molnár S. von, Roukes M. L., Chtchelkanova A. Y., Treger D. M. 2001 *Science* **294** 1488.
- [2] Žutić J., Fabian J., Sarma S.D. 2004 *Reviews of modern physics* **76** 323.
- [3] Ikeda S., Hayakawa J., Lee Y. M., Matsukura F., Ohno Y., Hanyu T. 2007 *IEEE Trans. Electron Devices* **54** 991.
- [4] Fert A. 2008 *Rev. Mod. Phys* **80** 41517.
- [5] Kent A., Worledge A. 2015 *Nat. Nanotechnol* **10** 187.
- [6] Sbiaa R., Piramanayagam S. N. 2017 *Phys. Status Solidi-RRL* **11** 1700163.
- [7] Sbiaa R., Law R., Lua S. Y. H., Tan E. L., Tahmasebi T., Wang C. C., Piramanayagam S. N. 2011 *Appl. Phys. Lett.* **99** 092506.
- [8] Sbiaa R., 2015 *J. Phys. D: Appl. Phys* **48** 195001.
- [9] Beach G. S. D., Nistor C., Knutson C., Tsoi M., Erskine J.L. 2005 *Nature Mater* **4** 741.
- [10] Jubert P.-O., Klau M., Bischof A., Rudiger U. Allenspach R. 2006 *J. Appl. Phys.* **99** 08G523.
- [11] Parkin S. S. P., Hayashi M. Thomas L. 2008 *Science* **320** 190.
- [12] O'Brien L., Read D. E., Zeng H. T., Lewis E. R., Petit D., Cowburn R. P. 2009 *Appl. Phys. Lett.* **95** 232502.
- [13] Moore T. A., Miron I. M., Gaudin G., Serret G., Auffret S., Rodmacq B., Schuhl A., Pizzini S., Vogel J., Bonfim M. 2008 *Appl. Phys. Lett.* **93** 262504.
- [14] Kim S.-R, Lee J.-Y., Choi Y.-S., Yu K. Guslienko, Lee K-S. 2008 *Appl. Phys. Lett.* **93** 052503.
- [15] Heyne L., Rhensius J., Bisig A., Krzyk S., Punke P., Kläui M., Heyderman L. J., Guyader L., Nolting F. 2010 *Appl. Phys. Lett.* **96** 032504.
- [16] Lahtinen T.H.E., Franke K.J.A., Van Dijken S. 2011 *Sci. Rep.* **2** 258.
- [17] Ueda K., Koyama T., Hiramatsu R., Chiba D., Fukami S., Tanigawa H., Suzuki T., Ohshima N., Ishiwata N., Nakatani Y., Kobayashi K., Ono T. 2012 *Appl. Phys. Lett.* **100** 202407.
- [19] Sbiaa R., Piramanayagam S. N. 2014 *Appl. Phys. A* **114** 1347.
- [20] Hayward T. J. 2015 *Sci. Rep.* **5** 13279.
- [21] Emori S., Umachi C. K., Bono D. C., Beach G. S. D. 2015 *J. Magn. Magn. Mat.* **378** 98.
- [22] Ai J., Miao B., Sun L., You B., Hu A., Ding H. 2011 *J. Appl. Phys.* **110** 093913.
- [23] Al Bahri M., Sbiaa R. 2016 *Sci. Rep.* **6** 28590.
- [24] Hayashi M., Thomas L., Rettner C., Moriya R., Jiang X., Parkin S. 2006 *Phys. Rev. Lett.* **97** 1.
- [25] Martinez E., Lopez-Diaz L., Torres L., Tristan C., Alejos O. 2007 *Phys. Rev. B - Condens. Mater. Phys.* **75** 1.
- [26] Noh S. J., Miyamoto Y., Okuda M., Hayashi N., Keun Kim Y. 2012 *J. Appl. Phys.* **111** 1.
- [27] Kunz A., Priem J. D. 2010 *IEEE Trans. Magn.* **46** 1559.
- [28] Ermolaeva O. L., Skorokhodov E. V., Mironov V. L. 2016 *Phys. Solid State* **58** 2223.
- [29] Al Bahri M., Borie B., Jin T. L., Sbiaa R., Klau M., Piramanayagam S. N. 2019 *Phys. Rev. Appl.* **11** 024023.
- [30] Al Subhi A., Sbiaa R. 2019 *J. Magn. Magn. Mater.* **489** 165460.
- [31] Thiaville A., Nakatani Y., Miltat J., Suzuki Y., 2005 *EPL* **69** 990.
- [32] Noh S. J., Tan R. P., Chun B. S. Kim Y. K. J. 2010 *Magn. Magn. Mater.* **322** 3601.
- [33] Fukami S., Suzuki T., Nakatani Y., Ishiwata N., Yamanouchi M., Ikeda S., Kasai K., Ohno H. 2011 *Appl. Phys. Lett.* **98** 082504.

- [34] Koyama T., Chiba D., Ueda K., Tanigawa H., Fukami S., Suzuki T., Ohshima N., Ishiwata N., Nakatani Y., Ono T. 2011 Appl. Phys. Lett. **98** 192509.
- [35] Sethi P., Krishnia S., Gan W., Kholid F., Tan F., Maddu R., Lew W. 2017 Sci. Rep. **7** 4964.
- [36] Ngo D. T., Ikeda K., Awano H. 2011 Appl. Phys. Express **4** 093002.
- [37] Khvalkovskiy A. V., Zvezdin K. A., Gorbunov Y. V., Cros V., Grollier J., Fert A., Zvezdin A. K. 2009 Phys. Rev. Lett. **102** 067206.
- [38] Girod S., Gottwald M., Andrieu S., Mangin S., McCord J., Fullerton E. E., Beaujour J.-M. L., Krishnatreya B. J., Kent A. D. 2009 Appl. Phys. Lett. **94** 262504.
- [39] Bandiera S., Sousa R. C., Rodmacq B., Dieny B. 2012 Appl. Phys. Lett. **100** 142410.
- [40] Akbulut S., Akbulut A., Özdemir M., Yildiz F. 2015 J. Magn. Magn. Mater. **390** 137.
- [41] Sbiaa R., Shaw J. M., Nembach H. T., Al Bahri M., Ranjbar M., Åkerman J., Piramanayagam S. N. 2016 J. Phys. D: Appl. Phys. **49** 425002.
- [42] Law W. C., Jin T. L., Zhu X. T., Nistala R. R., Thiyagarajah N., Seet C. S., Lew W. S. 2019 Magn J. Magn. Mater. **477** 124.
- [43] Malinowski G., Boulle O., Klaui M. 2011 J. Phys. D: Appl. Phys. **44** 384005.